ACS OMEGA

Open Access

http://pubs.acs.org/journal/acsodf

Article

Characterization of Chitosan-Hybridized Diatomite as Potential Delivery Systems of Oxaliplatin and 5-Fluorouracil Drugs: Equilibrium and Release Kinetics

Haifa E. Alfassam, Sarah I. Othman, May N. Bin Jumah, Maha A. Al-Waili, Ahmed A. Allam, Wail Al Zoubi,* and Mostafa R. Abukhadra*

Cite This: *ACS Omega* 2023, 8, 38330−38344

Read Online

ACCESS | Metrics & More | Article Recommendations

ABSTRACT: The current work involves the modification of diatomite's biosiliceous frustules employing chitosan polymer chains (CS/Di) to serve as low-cost, biocompatible, multifunctional, and enhanced pharmaceutical delivery systems for 5-fluorouracil (5-Fu) together with oxaliplatin (OXPL). The CS/Di carrier displayed strong loading characteristics, notably at saturation (249.17 mg/g (OXPL) and 267.6 mg/g (5-Fu)), demonstrating a substantial 5-Fu affinity. The loading of the two types of medications onto CS/Di was conducted based on the kinetic behaviors of the conventional pseudo-first-order theory (R^2 > 0.90). However, while the loading of OXPL follows the isotherm assumptions of the classic Langmuir model (R^2 = 0.99), the loading of 5-Fu displays Fruendlich isotherm properties. Therefore, the 5-Fu loading displayed physical, heterogeneous, and multilayer loading properties, whereas the loading of OXPL occurred in homogeneous and monolayer form. The densities of occupied active sites of CS/Di were 37.19 and 32.8 mg/g for the sequestrations of OXPL and 5-Fu, respectively. Furthermore, by means of multimolecular processes, each loading site of CS/Di can bind up to 8 molecules of OXPL and 9 molecules of 5-Fu in a vertical orientation. This observation explains the higher loading capacities of 5-Fu in comparison to OXPL. The loading energies, which exhibit values <40 kJ/mol, provide confirmation of the dominant and significant consequences of physical processes as the regulating mechanisms. The release patterns of OXPL and 5-Fu demonstrate prolonged features over a duration of up to 120 h. The release kinetic simulation and diffusion exponents which are more than 0.45 provide evidence of the release of OXP and 5-Fu via non-Fickian transportation characteristics and the erosion/diffusion mechanism. The CS/Di carrier exhibited a substantial enhancement in the cytotoxicity of OXPL and 5-Fu against HCT-116 carcinoma cell lines, resulting in a reduction in cell viability by 4.61 and 2.26% respectively.

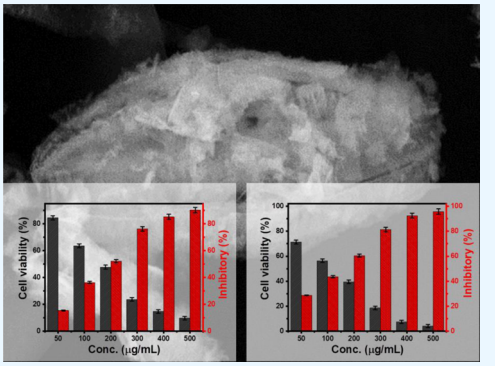

1. INTRODUCTION

Noncommunicable diseases, such as malignancies, are responsible for roughly 72% of reported death rates worldwide. Based on future projections, it is conceivable that there may be a 75% surge.[1,2] Colorectal cancer is a very widespread malignant disease, impacting roughly 13% of those diagnosed with cancer.[3,4] Colorectal cancer often arises from the growth of a polyp within the mucosal layers, eventually progressing to include the submucosal and nearby tissues. In the later phases of colorectal tumors, there is a discernible escalation in the proliferation of malignant cells inside the lymphatic system and adjacent organs.[5] Colorectal carcinoma has been identified as a major cause of the global death rates, hence posing a severe risk to human existence.[6,7] Therefore, health and research organizations have made it a priority to provide safe, cost-effective, and easily accessible modern treatments.[3,7] Chemotherapy is a highly effective and commonly used treatment method in the field of cancer therapy.[8] Chemotherapy approaches may elicit substantial oxidative stress or successfully impede DNA replication, hence resulting in the demise of malignant cells.[7,9] Unfortunately, the chemotherapeutic medicines often used in clinical practice might have detrimental effects on normal cells due to their nonselective properties.[3,10] The therapeutic regimen has the potential to induce adverse effects like renal hematologic suppression and malfunction, as well as symptoms of vomiting and nausea. Presently, there is quite a bit of scientific study being conducted to establish novel materials that possess the ability to serve as efficient carriers of pharmaceutical compounds. These materials have

Received: July 3, 2023
Accepted: September 21, 2023
Published: October 6, 2023

the potential to deliver drugs to specific sites, enhance therapeutic efficacy, and reduce undesired side effects.[11,12]

Chemotherapeutic agents like 5-fluorouracil (5-Fu) and oxaliplatin (OXPL) have been approved for the treatment of colorectal tumors.[13−15] The anticancer effects of OXPL on tumor cells are due to the creation of covalent bonds between its intracellular metabolites and DNA double strands. This process inhibits the replication and transcription of DNA.[4,16] The intracellular 5-Fu conversion produces cytotoxic chemicals that disrupt RNA synthesis and impair the action of thymidylate enzymes, which has a pivotal function in the production of DNA nucleotides known as thymidine.[17,18] The approval of OXPL and 5-Fu by the FDA as chemotherapeutic agents for the treatment of colorectal cancer necessitates consideration of the potential adverse impacts of these medications on healthy cells.[5,7,19] A number of investigations have documented the potential toxicities related to OXPL, including but not limited to oral mucosal irritation, emesis, neurotoxic symptoms, myotoxic impacts, gastrointestinal disturbances, and abnormalities in the gastrointestinal (GI) system.[20−22] Moreover, it has been established that the injection of 5-Fu medication induces cytotoxic effects in several physiological systems, such as the neurological, hematological, digestive tract, dermatological, and cardiovascular systems.[1,23] Consequently, numerous types of improved delivery methods have been investigated in an effort to regulate the release rates, mitigate the negative consequences, and increase both the specificity and curative effectiveness of 5-Fu and OXPL medications.[7,23,24]

Various categories of materials, involving inorganic compounds, such as mesoporous silica and modified hydroxyapatite, as well as organic counterparts like polymer chains, lipid nanoparticles, and alginate nanogels in addition to hybrid materials that blend organic and inorganic components, have been looked at as possible carriers for chemotherapy drugs.[7,22,24−27] Several factors, such as biocompatibility, loading capacity, nontoxicity, preparation cost, and release rate, must be considered when selecting an appropriate drug carrier.[28] Due to their high surface polarity, silica-based materials with mesoporous and microporous frameworks are highly sought after. This is because they make it easier for drugs to get into the bloodstream and increase the efficiency of drug loading.[29] Unfortunately, producing synthetic silica materials necessitates time-consuming and expensive synthesis processes. Furthermore, the synthesis process may involve the use of hazardous raw materials and byproducts.[28] To address the economic and environmental concerns described earlier, natural porous silicate and silica, such as diatomite, were employed as substitutes for synthesized materials.[30,31]

Diatomite, commonly known as diatomaceous earth, is a biologically generated type of natural sedimentary rock that may be readily acquired at a relatively cheap cost.[32,33] Diatomite mostly comprises amorphous silica, predominantly including well-preserved diatom frustules.[34,35] Both the unmodified and modified structures of diatomite have been evaluated as potential carriers for transferring small drugs and macromolecules, according to studies.[28,36−38] Numerous advantageous characteristics for drug carriers have been discovered to be present in diatomite, including high porosity, low density, nontoxicity, high loading capacity, thermal stability, mechanical stability, and chemical resistance.[16,28,39,40] To improve drug loading and release properties, as well as ensure safety, biodegradability, and biocompatibility, diatomite was functionalized or modified with various groups of chemicals, prevalent biopolymers, and nontoxic inorganic compounds.[32,38,41−43]

Chitosan, a well-established biopolymer, has significant importance in diverse fields, such as pharmaceuticals, environmental science, and medicine. Its primary use is in serving as a drug carrier.[28,44,45] Chitosan, a polyaminosaccharide polymer, has several technological advantages and may be readily synthesized from the chitin component of various biogenic resources.[44] Chitosan chains have notable advantages in terms of safety, hemostatic efficacy, biological activity, biological compatibility, and biodegradable properties alongside their commendable mechanical and adsorption characteristics.[28] As a result, this study describes the synthesis and characterization of a novel hybrid composite material (CS/Di) made of integrated polymeric chains of chitosan and diatomite (Di) that may be used as an effective, affordable, and biocarrier for anticancer drugs (5-fluorouracil (5-Fu) and oxaliplatin (OXPL)) with enhanced loading, release, and cytotoxic properties. By examination of the influencing experimental factors, representative kinetic assumptions, illustrative isotherm models, and thermodynamic behaviors, the loading of OXPL and 5-Fu was examined in light of the loading capacities and the influencing loading mechanisms. The release characteristics and kinetics were analyzed by assessing the experimental release findings and using a variety of in vitro release kinetic models. Furthermore, the anticancer properties of the CS/Di hybrid material (without medication) and the CS/Di preloaded with 5-Fu and OXPL were evaluated toward colorectal tumor cells by in vitro cytotoxic tests.

2. RESULTS AND DISCUSSION

2.1. Characterization. The X-ray diffraction (XRD) patterns of CS/Di, chitosan, and refined diatomite are shown in Figure 1A. A sizable diffraction peak at a 2θ angle of 22° is typically present with amorphous silica in diatoms (Figure 1A).[40] Commercial chitosan with semicrystalline characteristics is identified by the diffraction peaks at 2 angles of 10 and 22° (Figure 1B). The major peak of the diatomite powder is clearly visible in the XRD pattern of the CS/Di composite, which was slightly offset at almost 26° (Figure 1C).

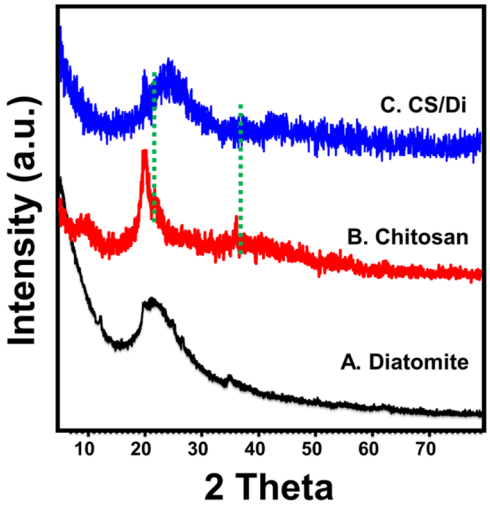

Figure 1. XRD patterns of raw diatomite (A), integrated chitosan (B), and synthetic CS/Di composite (C).

https://doi.org/10.1021/acsomega.3c04750
ACS Omega 2023, 8, 38330−38344

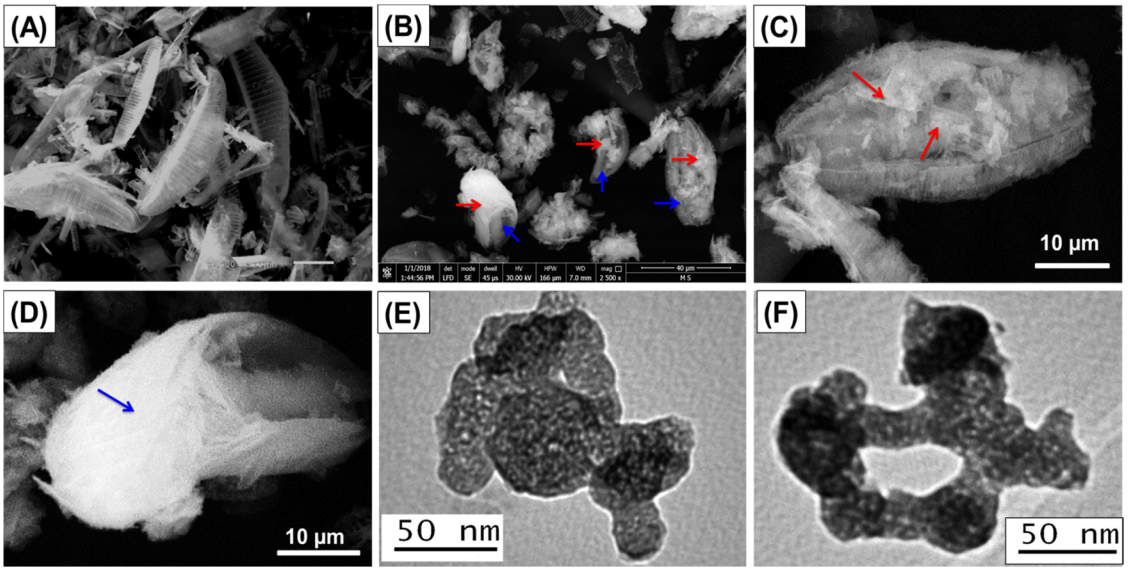

Figure 2. SEM images of raw diatomite (A), general SEM images for the diatomite particulate coated with the chitosan polymeric matrix (B,C), high magnification images for the chitosan matrix on the surface of diatomite particles (D, E), and HRTEM images of the synthetic CS/Di composite (E, F).

Furthermore, one of the two essential chitosan peaks was eliminated, while the remaining peak has been shifted and combined with the diatomite essential peak, ensuring an efficient combination between both diatomite precursors and the chitosan biopolymer.

Both the refined diatomite powder and the CS/Di composite's surface features have been studied by using scanning electron microscopy (SEM) and high-resolution transmission electron microscopy (HRTEM) images (Figure 2B−E). The diatomite granules have a pinnate-like form and are distinguished by a large number of painstakingly positioned pores that decorate their structures (Figure 2B). The surface characteristics of diatomite as frustules were modified strongly after the integration of chitosan, as seen in the SEM images of CS/Di (Figure 2C). The diatomite structures were partially, and occasionally totally, aggregated, and the chitosan chains gave the overall form a roughly spherical appearance (Figure 2C). A high-resolution image of the chitosan clusters reveals that they formed as nanofibers, which typically identify chitosan chains. The HRTEM images of the CS/Di material show that the diatomite granules were successfully trapped inside the tabulated chitosan chains that give the framework nanoporous features (Figure 2D,E). The chitosan tabular granules' interaction produced secondary nanopores as well, increasing the surface area of the overall structure, which has a significant impact on the loading properties of CS/Di (Figure 2D,E).

The previous morphological features were reflected in the textural properties of the composite as compared to the raw diatomite (Table 1). The CS/Di composite had a measured BET surface area of 162.4 m^2/g, whereas diatomite was measured to have a surface area of 117.7 m^2/g, which affects strongly on the loading behavior of the composite (Table 1).

The synthesis of the CS/Di composite was also validated by comparing its Fourier transform infrared (FTIR) spectrum to that of chitosan and diatomite (Figure 3). Diatomite's absorption spectra show distinct bands at 3437 cm^{-1} (Si−O−H), 465 cm^{-1} (Si−O), and 1638 cm^{-1} (adsorbed H−O−H) (Figure 3A).[40] Moreover, it may be inferred that the two

Table 1. Textural Characterization of Raw Diatomite and CS/Di Composite

	raw diatomite	CS/Di composite
BET surface area (m^2/g)	117.7	162.4
external surface area (m^2/g)	78	102.3
micropore surface area (m^2/g)	39.7	60.1
pore volume (cm^3/g)	0.032	0.071
average pore diameter (nm)	5.41	6.13

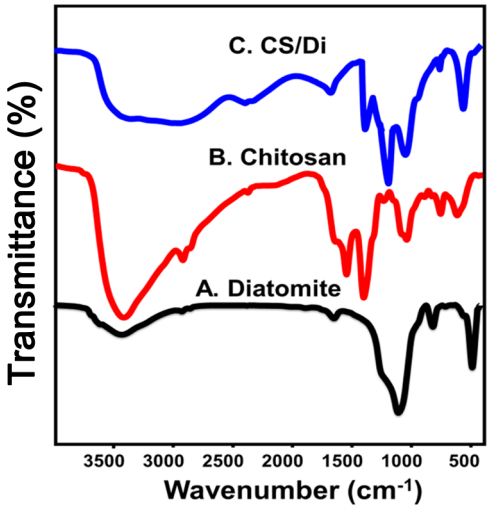

Figure 3. FTIR spectra of raw diatomite (A), chitosan (B), and synthetic CS/Di composite (C).

distinct peaks noticed at 799 and 1092 cm^{-1} correspond, respectively, to the symmetrical and asymmetrical vibrations of the Si−O−Si bonds (Figure 3A).[28] N−H (1547 cm^{-1}), C−O (1040 cm^{-1}), OH (3423 cm^{-1}), C−N (1402 cm^{-1}), C═O (1637 cm^{-1}), and C−H (2925 and 1336 cm^{-1}) were the principal bands that were distinguished in the spectrum of chitosan[28,44] (Figure 3B). Following a successful integration operation, the distinct CS/D spectrum shows a significant rise

https://doi.org/10.1021/acsomega.3c04750
ACS Omega 2023, 8, 38330−38344

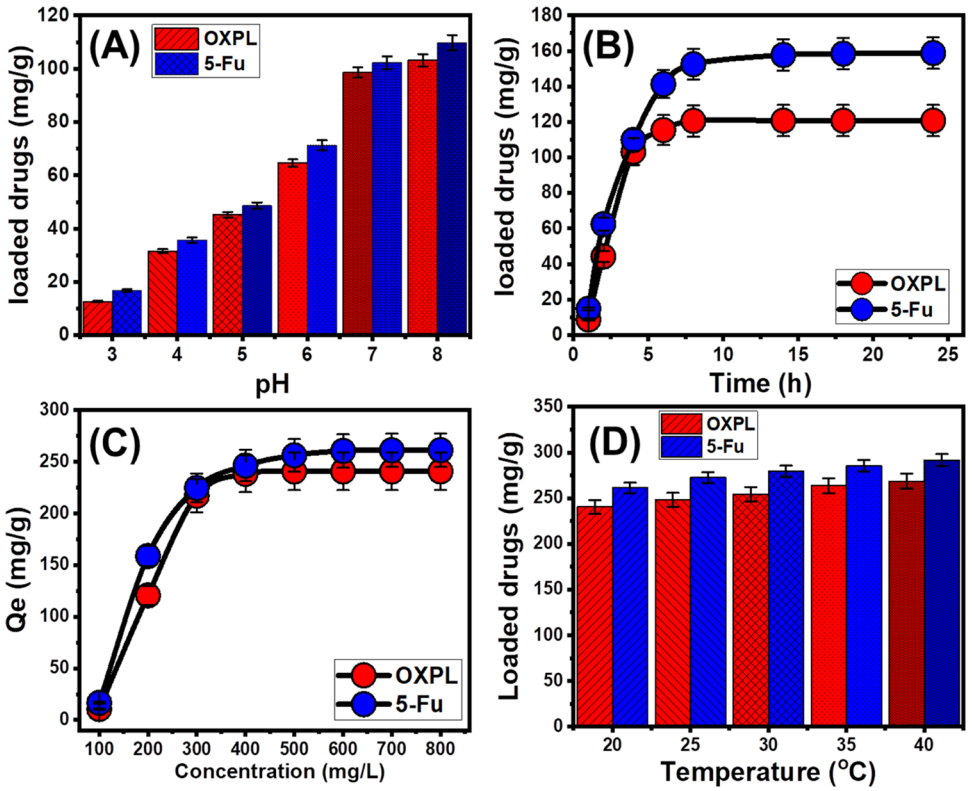

Figure 4. Experimental influence of the controlling variables on the actual loading behaviors of OXPL as well as 5-Fu using CS/Di, including (A) pH, (B) contact time, (C) starting concentrations, and (D) temperature.

in the principal amorphous silica band intensity at 3433 cm^{-1} as compared to the bands noticed for diatomite as one phase (Figure 3C). Furthermore, Si−O and Si−O−Si groups in shifted positions have been identified as other distinctive diatomite bands (Figure 3C). The composite also included the chitosan-specific bands C═O, C−N, and C−O, which have been detected by their offset positions (Figure 3C). The results verify the effective hybridization of diatomite with chitosan in the CS/Di composite.

2.2. Drug Loading Studies. *2.2.1. Effect of Experimental Factors. 2.2.1.1. pH.* The experimental adjustment of pH has a significant impact on the charge distribution on the surface of CS/Di as well as the speciation of OXPL and 5-Fu. Within a pH range of 3 to 8, the study assessed the influence of pH on performed loading tests of the two medications (Figure 4A). The other loading parameters, including the loading temperature (20 °C), the loading period (6 h), the OXPL or 5-Fu concentrations (200 mg/L), the solution volume (50 mL), and the CS/Di dosage (20 mg), were all maintained at precise values. The results show a steady improvement in successful drug loading capacities as the pH values increase from 3 to 8 (Figure 4A). The highest drug loading capabilities have been observed at a pH of 8 (109.8 mg/g (5-Fu) and 103.2 mg/g (OXPL)). The predominant surface charges of CS and Di and the ionization states of the medicines are responsible for the reported results. The OXPL species are very mobile and soluble in acidic environments. Furthermore, the most abundant species of OXPL ions have a positive charge ($[Pt(dach)(H_2O)Cl]^+$ and $[Pt(dach)(H_2O)_2]^{2+}$) that demonstrates electrostatic repulsive behevior against the positively energized surfaces of the CS/Di particulates.[46,47] Furthermore, the process of ionization of 5-Fu medicines is enhanced at elevated pH levels, resulting in increased movement of the medication ions and subsequent electrostatic interaction with the negatively energized outermost layer of the CS/Di carrier.[23] These findings were supported by the determined values of $pH_{(PZC)}$ for the composite during the uptake of 5-Fu (pH 6.7) and OXPL (pH 7.2) molecules, which declare the enrichment of the surface of the composite with numerous sites at the pH conditions higher than these pH values.

2.2.1.2. Loading Duration. The influence of loading duration was evaluated within an extended interval of 1 until 24 h to find the required interval to attain the maximal capacity and to ascertain the states of equilibrium (Figure 4B). All other loading factors were held constant throughout the experiment, with the assessed concentration set at 200 mg/L, the initial pH kept at 8, the total volume set at 50 mL, the CS/Di dose at 20 mg, and the temperature kept at 20 °C. The progressive prolongation of the loading time led to notable augmentations in the amount of 5-Fu and OXPL that were loaded onto the CS/Di material (Figure 4B). The improvement of drug-loaded quantities may be recognized over a duration of up to 12 h for OXPL as well as for 5-Fu. Beyond this interval, the amounts of the medication ions that have been loaded demonstrate a limited or constant variation, revealing that the equilibrium states of CS/Di nanoparticles have been attained (Figure 4B). At the start of the loading procedure, numerous active receptors were easily accessible, which is what led to the observable rise in the medication-loaded amounts at very rapid rates. The sustained use of those receptors with the medication ions over a prolonged duration led to a gradual decline in their uptake rates until the receptors had been fully depleted. This behavior reduces the potential for additional loading and

https://doi.org/10.1021/acsomega.3c04750
ACS Omega 2023, 8, 38330−38344

establishes the equilibrium capacities of CS/Di (OXPL (120.7 mg/g) or 5-Fu (158.8 mg/g)).[48]

2.2.1.3. Drug Concentration. OXPL and 5-Fu loading experiments were performed with an incremental increase in drug concentrations (100−800 mg/L) to evaluate the highest potential loading capacities of CS/Di. The primary loading settings were held constant throughout the experiment. These conditions included a pH value of 8, a 50 mL solution, a loading duration of 24 h, a dose of 20 mg, and a temperature of 20 °C. The findings show that increasing the concentrations that were investigated up to 400 and 600 mg/L significantly improved the loading capacity of CS/Di for OXPL and 5-Fu (Figure 4C). In some investigations, this loading tendency has been attributed to the anticipated increase in driving forces of drugs at elevated concentrations. The corresponding rise in the driving factors enables the transportation and the transfer of the medication ions within the bulk solutions toward the accessible loading sites on CS/Di, hence augmenting its capacities for loading.[28,49] The loading efficiencies of CS/Di showed little to no augmentation at the examined concentrations beyond 600 mg/L (5-Fu) and 400 mg/L (OXPL), which are the equilibration concentrations (Figure 4C). The greatest loading capacities of CS/Di for 5-Fu (261.3 mg/g) and OXPL (240.8 mg/g) can be determined at equilibrium concentrations, which are specified as the concentrations at which all loading receptors of CS/Di become completely occupied by drug ions.

2.2.1.4. Temperature. The drug loading studies were performed by gradually increasing the temperature from 20 to 40 °C in an ongoing manner (Figure 4D) to ascertain whether the temperature supported or hindered the loading efficiency of CS/Di. At 24 h (duration), 800 mg/L (5-Fu or OXPL concentrations), 20 mg (the dosage), pH 8 (the loading pH), 50 mL (the total volume), and 20 °C (loading temperature), the loading variables were adjusted. The loading characteristics of CS/Di for the medications increase as the testing temperature increases, demonstrating endothermic mechanisms (Figure 4D). The measured loading capacities for OXPL and 5-Fu at 40 °C are 268.6 and 291.8 mg/g, respectively (Figure 4D). The CS/Di composite has attractive qualities as a carrier for OXPL and 5-Fu as a consequence of its high loading characteristics, according to the findings of loading studies. In addition, the adjustment of the principal loading parameters, such as pH, time, concentration, and temperature, enables the control of drug quantities loaded into CS/Di.

2.2.2. Loading Mechanism. 2.2.2.1. Kinetic Studies. 2.2.2.1.1. Intraparticle Diffusion Behavior. To determine what influences loading mechanisms, the intraparticle diffusion behaviors of the two medications loaded onto CS/Di have been assessed (Figure 5). The established curves display multilinear (segmental) features that do not cross over at the origin. The results of OXPL and 5-Fu loading provide verification that the loading activities onto CS/Di are controlled by multistep regulating mechanisms, more than just the intraparticle diffusion process.[50] The curves obtained for two tested medications demonstrate that three consecutive controlling stages—exterior adsorption, intraparticle diffusion, and saturating phases—occurred throughout the loading activities (Figure 5).[51] The outer surface adsorption stage is represented by the first noticeable segment. This step is primarily impacted by the availability of the reactive receptors on the CS/Di surface.[52] The subsequent stage corresponds to

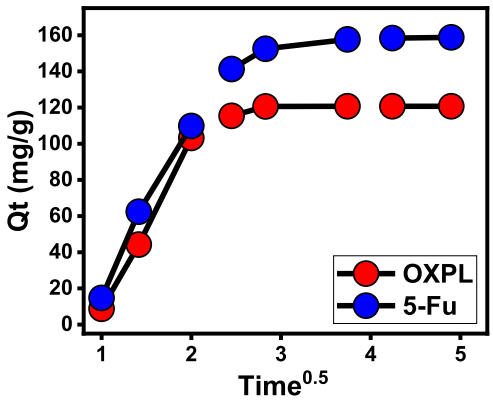

Figure 5. Recognized OXPL and 5-Fu loading intraparticle diffusion curves by CS/Di.

the intraparticle diffusion phases, when drug ions diffuse into the inside pores of the CS/Di material, adsorbing onto the interior loading receptors with little involvement by the outside loading receptors (Figure 5).[52] The equilibration and saturation stages, which make up the third and last segments, demonstrate a minimal to nonexistent improvement in the loading capacities of CS/Di for the two drugs under consideration. The achievement of equilibrium phases may be ascribed to the fully saturated state of all loading sites and the formation of densely overloaded layers comprising the medication onto the surface of CS/Di via molecular interactions in addition to interionic attractions.[49,52]

2.2.2.1.2. Kinetic Modeling. The mathematical parameters and hypotheses of the pseudo-first-order (PFO) (eq 1) and pseudo-second-order (PSO) (eq 2) models were used to investigate the kinetics of the loading activities of OXPL and 5-Fu onto CS/Di. The nonlinear fitting process was employed to determine the fit degrees based on the calculating determination coefficient (R^2) and chi-square (X^2) (Figure 6A,B and Table 2).[28]

$$Q_t = Q_e(1 - e^{-k_1 \cdot t}) \quad (1)$$

$$Q_t = \frac{Q_e^2 k_2 t}{1 + Q_e k_2 t} \quad (2)$$

The loading methods of 5-Fu as well as OXPL onto CS/Di exhibit a higher degree of consistency with the evaluated PFO model (Figure 6A,B and Table 2). The resulting convergence of the greatest hypothetical loading qualities of CS/Di, as determined via the PFO model (172.9 mg/g (5-Fu) and 135.03 mg/g (OXPL)) with the highest values measured in experiments (158.8 mg/g (5-Fu) and 120.7 mg/g (OXPL)) provides support for this kinetic conclusion. The significance of the physical reactions, such as the electrostatic attractions during OXPL and 5-Fu loading onto CS/Di, has been emphasized by the fitting of PFO over PSO.[22] However, the PSO formula also closely matched the outcomes of the two medications, validating that a few minor chemical interactions (complexation, hydrophobic interactions, and hydrogen bonding) had a considerable impact during the loading activities.[28]

2.2.2.2. Equilibrium Properties. 2.2.2.2.1. Classic Isotherm Modeling. Three conventional isotherm models—Langmuir (eq 3), Freundlich (eq 4), and Dubinin−Radushkevich (D−R) (eq 5) models—were used to evaluate the equilibrium

https://doi.org/10.1021/acsomega.3c04750
ACS Omega 2023, 8, 38330−38344

Table 2. Determined Mathematical Factors of the Addressed Models, Including Kinetics, Conventional Equilibrium, Advanced Equilibrium, Thermodynamics, and Release Kinetics

models	parameters	OXPL	5-Fu
	Kinetic Models		
pseudo-first-order	K_1 (min^{-1})	0.182	0.193
	$Q_{e(Cal)}$ (mg/g)	135.03	172.9
	R^2	0.89	0.93
	X^2	7.1	4.49
pseudo-second order	K_2 (g mg^{-1} min^{-1})	7.58×10^{-4}	56.74×10^{-4}
	$Q_{e(Cal)}$ (mg/g)	184.4	230.9
	R^2	0.84	0.90
	X^2	8.9	6.3
	Classic Isotherm Models		
Langmuir	Q_{max} (mg/g)	250.7	282.4
	b (L/mg)	3.11×10^{-5}	5.72×10^{-8}
	R^2	0.99	0.98
	X^2	0.04	0.74
	R_L	0.99	0.99
Freundlich	$1/n$	0.27	0.21
	K_F (mg/g)	247.6	256.3
	R^2	0.98	0.99
	X^2	0.88	0.26
D−R model	β (mol^2/KJ^2)	0.01528	0.0133
	Q_m (mg/g)	288	294.6
	R^2	0.96	0.94
	X^2	5.9	7.0
	E (kJ/mol)	5.72	6.12
monolayer model of one energy	n	6.7	8.17
	N_m (mg/g)	37.19	32.8
	$Q_{(sat)}$ (mg/g)	249.17	267.9
	ΔE (kJ/mol)	−8.94	−11.08
	Thermodynamics		
$\Delta G°$ (kJ/mol)	293.15	−7.98	−8.20
	298.15	−8.21	−8.21
	303.15	−8.42	−8.42
	308.15	−8.67	−8.67
	313.15	−8.87	−8.87
$\Delta H°$ (kJ/mol)		5.12	5.05
$\Delta S°$ (J K^{-1} mol^{-1})		44.7	45.14

release kinetic models				
determination coefficient (R^2)				
	OXPL		5-Fu	
models	acetate buffer (pH 5.5)	phosphate buffer (pH 7.4)	gastric fluid (pH 1.2)	intestinal fluid (pH 7.4)
zero-order model	0.80	0.86	0.84	0.76
first-order model	0.98	0.96	0.96	0.97
Higuchi model	0.95	0.98	0.97	0.93
Hixson−Crowell model	0.98	0.96	0.93	0.98
Krosmeyer−Peppas model	0.91	0.90	0.95	0.92
n	0.62	0.75	0.69	0.56

properties of the OXPL and 5-Fu loading mechanisms onto CS/Di. R^2 and X^2 values were identified using nonlinear fitting as the basis to determine the degree of fit (Figure 6C,D and Table 2).

$$Q_e = \frac{Q_{max} b C_e}{(1 + bC_e)} \quad (3)$$

$$Q_e = K_f C_e^{1/n} \quad (4)$$

$$Q_e = Q_m e^{-\beta \varepsilon^2} \quad (5)$$

The values of R^2 and X^2 show that, compared to the Freundlich model, the Langmuir isotherm hypothesis more accurately describes the results of the loading mechanisms of OXPL onto CS/Di. This finding demonstrates that homogeneous and monolayer loading represents the majority of the OXPL and 5-Fu loading processes.[53] The 5-Fu loading process exhibits the Freundlich model's isotherm features, which point to the heterogeneous and multilayer loading of its ions onto CS/Di. Additionally, the Langmuir model's expected values of RL (the equilibration factor) are <1, showing that the two medications have favorable features onto CS/Di (Figure 6C,D

https://doi.org/10.1021/acsomega.3c04750
ACS Omega 2023, 8, 38330−38344

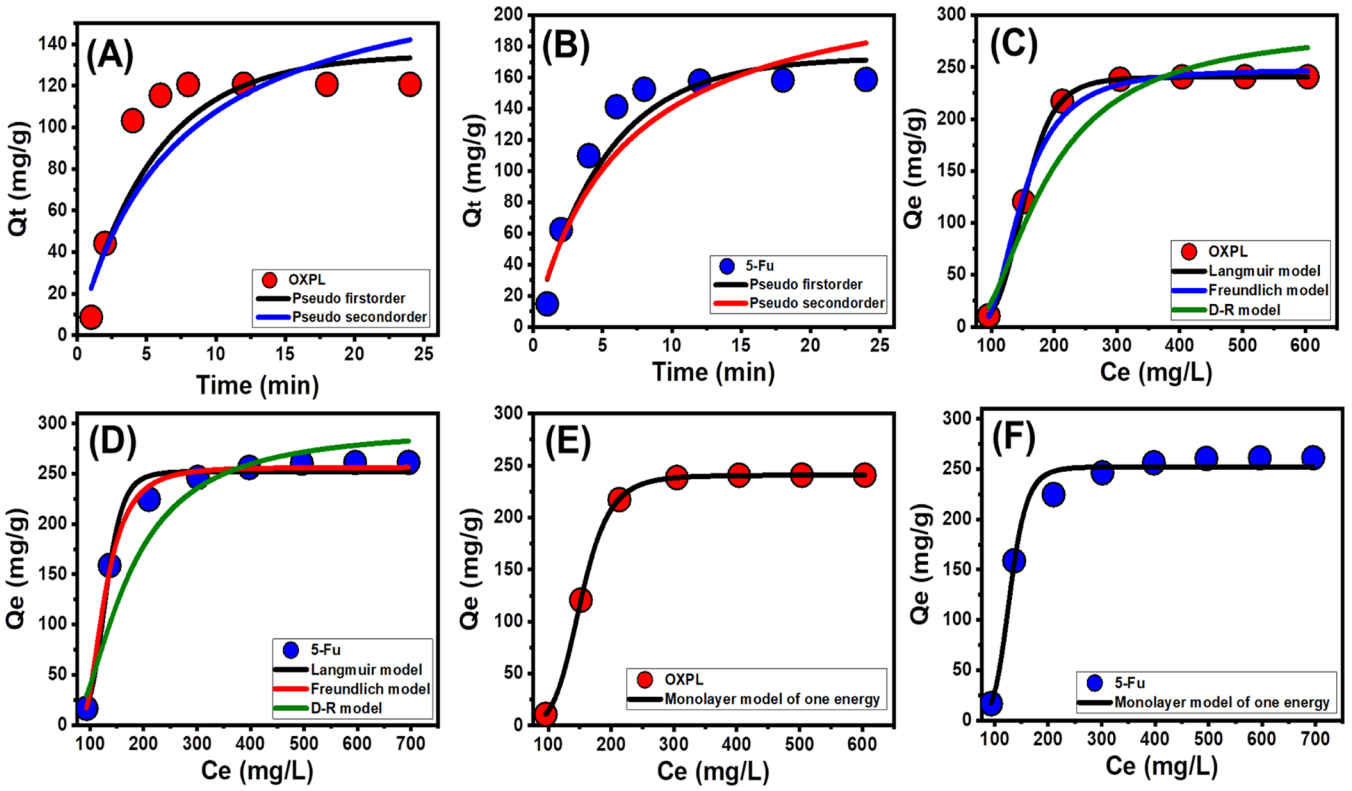

Figure 6. Kinetic modeling of the OXPL (A), 5-Fu (B) loading behaviors (A), equilibrium modeling of the OXPL (C) and 5-Fu (D) loading properties based on the classic isotherm models, and advanced equilibrium modeling of OXPL (E) and 5-Fu (F) loading behaviors according to the monolayer model of one energy.

and Table 2). According to the Langmuir equilibrium analysis, the anticipated maximal loading capacities (Q_{max}) of 5-Fu and OXPL are 282.4 and 250.7 mg/g, respectively.

The D−R isotherm is particularly promising in revealing the energetic heterogeneity of CS/Di during the loading activities of medications, irrespective of the reported homogeneity or heterogeneity of its surface.[54] The D−R model's Gaussian energy (E), which is obtained mathematically, provides an essential function in identifying the type of mechanisms that were participating during the encapsulation of OXPL as well as 5-Fu, whether they are physical or chemical in origin.[54,55] Strong physical processes are operating when E values are less than 8 kJ/mol, while mild chemical or complex physical and chemical processes are operating when E values are between 8 and 16 kJ/mol. E values of over 16 kJ/mol for loading processes are a sign of strong chemical mechanisms. The established values of E for both loading activities are 5.72 kJ/mol (OXPL) and 6.12 kJ/mol (5-Fu) (Table 2). As the E values are <8, physical mechanisms dominate the loading of the two medications onto CS/Di.[55]

2.2.2.2.2. Advanced Equilibrium Studies. On the basis of statistical physics, advanced isotherm (equilibrium) models have been studied to ascertain how OXPL and 5-Fu are loaded onto CS/Di. The representative model for fitting the two medication loading findings (Figure 6E,F and Table 2) was the monolayer model of one energy site (eq 6), which had the highest R^2 and lowest root-mean-square error (RMSE).

$$Q = nN_o = \frac{nN_m}{1 + \left(\frac{C_{1/2}}{C_e}\right)^n} = \frac{Q_o}{1 + \left(\frac{C_{1/2}}{C_e}\right)^n} \quad (6)$$

The monolayer models of one energy site's mathematical parameters were established in order to clarify the overall loading mechanisms. The energetic (loading energy (E)) and steric (loading site density (N_m), number of sequestrated ions per single site (n), and saturation drug loading capacities (Q_{sat})) parameters are displayed in Table 2. For OXPL and 5-Fu, the Nm values of CS/Di are 37.19 and 32.8 mg/g, respectively (Table 2). Moreover, OXPL and 5-Fu ions can be loaded onto CS/Di with calculated n values over 1 (n = 6.7 (OXPL) and 8.17 (5-Fu)) (Table 2). These imply that about 7 to 8 atoms of OXPL and 8 to 9 atoms of 5-Fu are adsorbable per active receptor on the outer surface of CS/Di. This explains why CS/Di has a higher experimental capacity for 5-Fu (267.9 mg/g) compared to that of OXPL (249.17 mg/g). Additionally, detecting a value of n larger than 1 demonstrates the multi-ionic interaction that occurs between the 5-Fu as well as OXPL ions and CS/Di loading sites, in addition to both the vertical orientations of the already loaded drug ions.[56,57] Using eq 7, the loading energies (E) were determined to establish the type of loading mechanisms that influence the loading of the two medications onto CS/Di.

$$\Delta E = -RT \ln\left(\frac{S}{C_{1/2}}\right) \quad (7)$$

The loading energies of CS/Di are −8.94 (OXPL) and −11.08 kJ/mol (5-Fu) (Table 2), respectively. According to the previously stated values, physical loading mechanisms relating to van der Waals forces (4 to10 kJ/mol), dipole bond forces (E = 2 to 29 kJ/mol), electrostatic attractive forces (2 to 50 kJ/mol), and hydrogen bonds (E < 30 kJ/mol) were suggested for the loading of 5-Fu and OXPL into CS/Di.[56,57]

https://doi.org/10.1021/acsomega.3c04750
ACS Omega 2023, 8, 38330−38344

2.2.2.3. Thermodynamic Studies. The thermodynamic tests for the two medications were followed from 20 °C until 40 °C. The loading conditions have been selected: pH 8, a concentration of 800 mg/L, a dose of 20 mg, and a solution volume of 50 mL. The study addressed enthalpy (ΔH°), Gibbs free energy (ΔG°), and entropy (ΔS°) as the essential functions of the thermodynamic systems. The van't Hoff eq (eq 8) was subjected to linear regression analysis to determine the values of ΔH° and ΔS°, while the values of ΔG° were estimated using eq 9[28] (Figure 7 and Table 2).

$$\ln(K_c) = \frac{\Delta S^{\circ}}{R} - \frac{\Delta H^{\circ}}{RT} \quad (8)$$

$$\Delta G^{\circ} = -RT \ln K_c \quad (9)$$

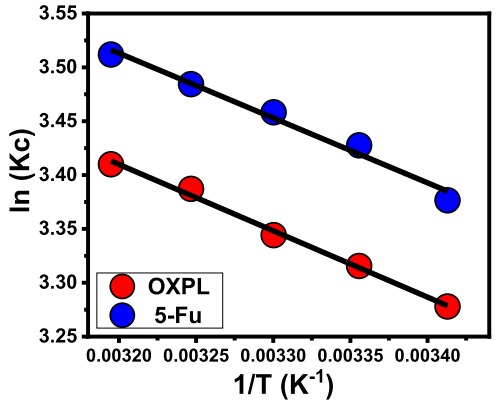

Figure 7. Linear regression agreement between the loading behaviors of the two medications and van't Hoff equation.

The results show that the loading of the two medications by CS/Di as a chemical has negative ΔG° values, revealing that these processes occurred spontaneously and are thermodynamically favorable (Table 2). The determined values of ΔH° are positive, revealing that the loading processes of the two medications onto the CS/Di particulates are endothermic in nature. The increase in temperature value results in a rise in the randomness of the OXPL and 5-Fu loading reactions, which is specified by the positive signs of ΔS° values.

2.3. In Vitro Release Profiles. To analyze the in vitro release profiles of the loaded OXPL ions from CS/Di, the percentages of the diffused ions within two buffering solutions (acetate buffer (pH 5.5) and phosphate buffer (pH 7.4)) were determined (Figure 8A). The selection of pH 5.5 and pH 7.4 has been made for the depiction of the environment close to mildly acidic cancer cells and body fluid, respectively.[58] Additionally, 5-Fu in vitro release assays were carried out within two chemical fluids (gastric fluid (pH 1.2) in addition to intestinal fluid (pH 7.4); Figure 8B). The established releasing percentages of the two medications within the assessed fluids exhibit clear variations in their rates of release as the duration passes (Figure 8). Both the rate of release of the OXPL and 5-Fu nanoparticles display an initially fast release that is followed by a slow but steady decrease over time until they reach the point of equilibrium release (Figure 8). OXPL and 5-Fu are released at faster rates during the early stages of the release duration, which can be ascribed to the feasible desorption of these molecules that were physically loaded onto the porous surfaces of CS/Di by weak mechanisms.[6,22] The release of the two medications retained inside the inner functional micropores of the diatomite carrier along with the coated matrix of CS might be the cause of a delay in the release rates with extended release times.[59,60]

The pH 5.5 induces the release speed of the OXPL release as compared to pH 7.4 (Figure 8A). It is believed that the higher mobility and significant solubility of OXPL's compound in acidic pH environments promote the release efficiency at pH 5.5.[46] In a pH 5.5 buffer, OXPL is slowly released from CS/Di, and the complete release status is attained after 120 h (Figure 8A). OXPL progresses gently for 120 h in pH 7.4 buffer without attaining the stage of full release (Figure 8A). 50% of the loaded OXPL had been released after 16 and 30 h at pH 5.5 and 7.4 (Figure 8A). After about 120 h at pH 5.5 and 7.4, the highest OXPL release percentages were 100 and 88.3%, respectively (Figure 8A). In contrast to pH 1.2, the release of 5-Fu occurs at a faster rate within the pH 7.4 buffer (Figure 8B). In basic conditions, the ionized state of 5-Fu molecules facilitated their transport and solubility. This was thought to be the cause of the higher amounts of 5-Fu released at a pH of 7.4.[29,61] The 5-Fu release progresses slowly for 120 h in the pH 1.2 fluid prior to completing the stage of equilibrium release (Figure 8B). After 120 h of 5-Fu release within the pH 7.4 buffer, the complete 5-Fu release state is attained (Figure 8B). According to the findings, about 50% of the dose of 5-Fu had been released within 30 h (pH 1.2) and 12 h (pH 7.4) (Figure 8B). In pH 1.2 solutions and pH 7.4 solutions, the maximum 5-Fu release percentages are 84.3 and 100%, respectively

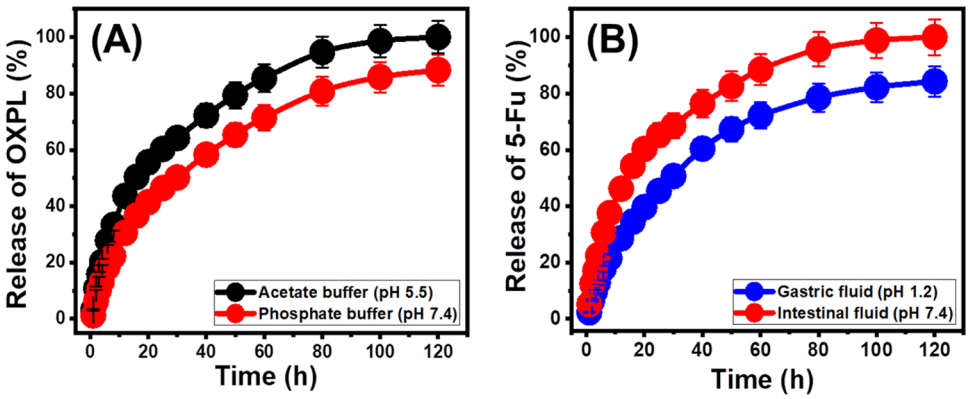

Figure 8. Experimental in vitro release properties of the composite as the carrier of (A) OXPL and (B) 5-Fu (OXPL (pH 5.5 and 7.4) and 5-Fu (pH 1.2 and 7.4)).

https://doi.org/10.1021/acsomega.3c04750
ACS Omega 2023, 8, 38330−38344

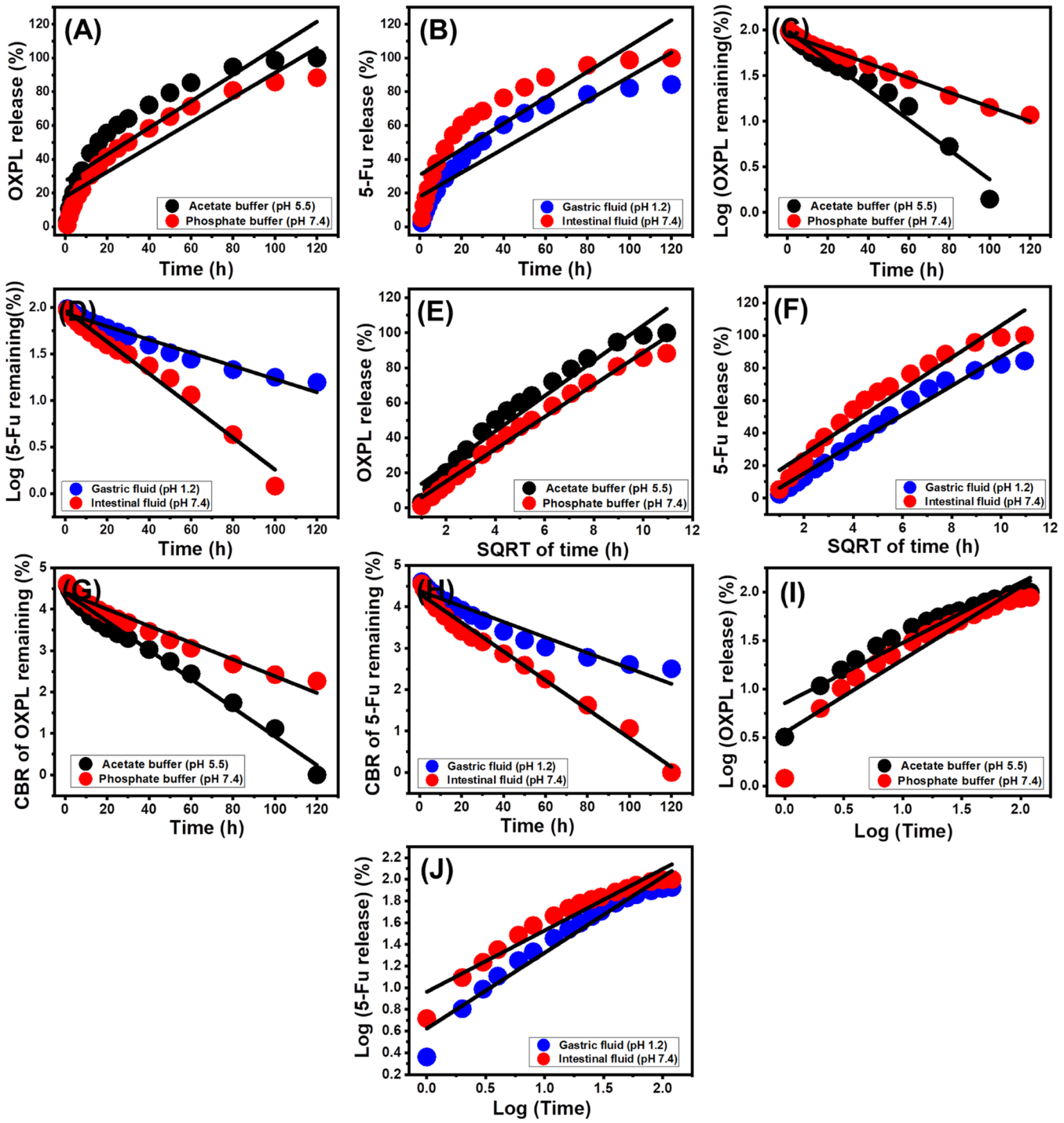

Figure 9. Linear regression fitting processes with zero-order ((A) OXPL and (B) 5-Fu), first-order ((C) OXPL and (D) 5-Fu), Higuchi ((E) OXPL and (F) 5-Fu), Hixson–Crowell ((G) OXPL and 5-Fu (H)), and Korsmeyer–Peppas ((I) OXPL and (J) 5-Fu) release models.

(Figure 8B). Drug carriers that deliver chemotherapy drugs to tumor cells via continuous release have proven effective as pharmaceuticals keep in contact with the diseased cells for a long time.[7,62] The hybrid chitosan polymer and diatomite-based organic/inorganic composite (CS/Di) that was utilized in the study show promising properties as a medication delivery system for the two medications. This is a result of its strong loading capacity in addition to the regulated release characteristics based on the applied ratios of the incorporated chitosan polymer during the synthetic procedure.

2.4. In Vitro Release Kinetics. The kinetic characteristics of the releasing processes are of great importance to establish the basic release mechanisms. The linear equations describing the kinetics of different models, such as the zero-order (eq 10), first-order (eq 11), Higuchi model (eq 12), Hixson–Crowell model (eq 13), and Korsmeyer–Peppas model (eq 14), were linearly fitted to the in vitro release results.

$$W_t - W_0 = K_0 \cdot t \tag{10}$$

$$\ln(W_\infty / W_t) = K_1 \cdot t \tag{11}$$

https://doi.org/10.1021/acsomega.3c04750
ACS Omega 2023, 8, 38330−38344

$$W_t = K_h t^{1/2} \quad (12)$$

$$W_o^{1/3} - W_t^{1/3} = K_{HC} t \quad (13)$$

$$W_t/W_\infty = K_p t^n \quad (14)$$

Drug release activities that display zero-order kinetics possess a fixed rate of diffusion or release, which is not influenced by the total amount of loaded medication.[6] Pharmaceutical processes controlled by first-order kinetics exhibit a notable dependency on the quantity of medication that has been previously supplied.[1] Drug diffusion is the primary release mechanism involved in drug release systems that adhere strongly to the Higuchi model.[1,62] The Higuchi model proposes some essential concepts, such as (A) the constant nature of the loaded medication's diffusion along alone direction, (B) the existence of a significantly greater medication dose versus its solubility, (C) the minimal influence of the solubility and swelling behaviors of the carriers, (D) the persistence of adequate sink characteristic, and (E) substantial differences between the size of the illicit drugs and the wall thickness of their carriers.[6] The Hixson−Crowell model-based release systems state that the drug release mechanisms are significantly influenced by the dimension and surface area of the carriers as well as the erosion processes.[28] The Korsmeyer−Peppas model can be applied to describe drug release from a polymer-based delivery system.[63] The kinetic outcomes of the Korsmeyer−Peppas model indicate that the coordinated diffusion and erosion mechanisms regulate drug release reactions.[1,22]

The first-order kinetics (Figure 9C,D and Table 2) have been identified to describe the release kinetics of the two addressed medications from CS/Di more perfectly than the kinetics of the zero-order model (Figure 9A,B and Table 2). The loading drug dosages significantly affected the release quantities of the two medications in all buffers tested. Excellent R^2 values can be observed during the fitting of the results with Higuchi (Figure 9E,F and Table 2) as well as Hixson−Crowell models (Figure 9G,H and Table 2). These results imply that collaboration between diffusion and erosion processes is the main factor affecting the release reactions of OXPL and 5-Fu. The implementation of the Korsmeyer−Peppas model, which showed a substantial level of compatibility with the release findings (Figure 9,J and Table 2), confirms the successful operation of the cooperative erosion/diffusion release mechanisms. The numerical values of the diffusional exponent (n), according to Korsmeyer−Peppas modeling, can be used as evidence of the mechanisms that are influencing the release activities of OXPL and 5-Fu. The n values that were obtained during the release of OXPL (0.62 (pH 5.5) and 0.75 (pH 7.4)) as well as of 5-Fu (0.69 (pH 1.2) and 0.56 (pH 7.4)), validating non-Fickian transportation of the two medications. Therefore, coordinated diffusion and erosion processes controlled the release mechanisms of OXPL and 5-Fu.

2.5. Comparative Study. The determined loading capacities and release profiles of CS/Di as potential carriers of both the OXPL and 5-Fu drugs were compared with those of other investigated carriers in the literature (Table 3). Regarding the loading capacity, the synthetic CS/Di composite displays enhanced loading properties either for OXPL or 5-Fu as compared to raw diatomite as well as most of the investigated structures in the literature (Table 3). Regarding the release profiles of the CS/Di composite, it displays significant slow release profiles considering the determined release profiles of the other studies. Its 5-Fu release profiles are considerably slower than those of most of the presented carriers (Table 3). However, the release profile of OXPL is faster than that of the compared carriers, but the structure still exhibits slow behavior for up to 100 h and might be increased as the highest release percentage after 100 h at pH 7.4 is 88.3%.

Table 3. Comparison between the Loading and Release Properties of the CS/Di Composite and Other Investigated Carriers in the Literature

carrier	loading capacity (mg/g)	release period (h)	references
	OXPL		
hydroxyapatite	49.1		64
cellulose/zeolite-A	285.7	150	65
zeolite-A	109.03	150	65
β-cyclodextrin/phillipsite	291.5	180	22
phillipsite	79.6	180	22
β-cyclodextrin/diatomite	238.7	120	66
diatomite	65.9	200	67
CS/Di	249.17	120	this study
	5-Fu		
montmorillonite/magnetite	59.44	24	68
HY zeolite	110	5	69
kaolinite nanotubes	103	60	48
chitosan/MCM-48	191	80	60
clinoptilolite	138.9	150	6
zeolite-A	134.2	100	69
chitosan/zeolite-A	218.2	100	69
diatomite	83.4	160	this study
CS/Di	267.6	120	this study

2.6. Cytotoxicity Properties. The study used freshly derived colorectal tissue cells (CCD-18Co) and cells from colorectal carcinoma (HCT-116) to assess the cytotoxicity of free CS/Di as well as its OXPL and 5-Fu preloaded compounds. Considering the expected experimental limit of the investigated doses, which spans from 20 to 120 μg/L, the observed cytotoxic impacts of CS/Di free particulates on the studied healthy CCD-18Co cell lines establish considerable biosafety characteristics, recommending their qualification as a delivery structure. The measured cell viability percentage of fresh cells after exposure to CS/Di at the highest dose (120 μg/L) is 94.2%. For HCT-116 cells that were treated with CS/Di as separate particulates, the results reveal substantial cytotoxic impacts, especially at evaluated dosages beyond 50 μg/mL. The cell viability had been determined to be 86.8%, demonstrating that the use of CS/Di as a free carrier inhibits the proliferation of cancer cells by 13.2%. In comparison to the free OXP and 5-Fu medicines, the loaded formulations show better performance in terms of cytotoxic influences and anticancer activities when applied to the HCT-116 tumor cell lines. The cell viability of CS/Di preloaded with the OXPL medication (500 μg/L) was 4.61%, the inhibitory % was 95.39%, and the IC-50 value was 11.23 μg/L. The findings pertaining to 5-Fu-preloaded CS/Di were observed to be the following: a cell viability of 2.26%, inhibition of 97.74%, and an IC-50 value of 5.72 μg/L.

https://doi.org/10.1021/acsomega.3c04750
ACS Omega 2023, 8, 38330−38344

3. CONCLUSIONS

Diatomite-functionalized chitosan (CS/Di) was studied as a promising delivery structure for two medications (OXPL and 5-Fu). As a suggested carrier, the CS/Di hybrid displays a notably significant loading capacity (249.17 mg/g (OXPL) and 267.6 mg/g (5-Fu)), and these capacities can be regulated effectively based on the operating conditions. Additionally, the structure exhibits notable sustained and extended release characteristics of OXPL and 5-Fu over a duration of about 120 h, which can provide prolonged and continuous exposure of tumor cells to the drug molecules. The loading of 5-Fu occurred in heterogeneous and multilayer form, while the loading of OXPL occurred in homogeneous and monolayer form based on the equilibrium assumptions (Langmuir (OXPL) and Freundlich (5-Fu)). Based on the D−R modeling, thermodynamic investigation, and loading energies, the two medications had been loaded physically in vertical arrangement by multimolecular processes on the surfaces of CS/Di. The kinetic modeling of the released activities demonstrates the non-Fickian transportation of the two medications by both erosion and diffusion reactions. The carrier significantly strengthens the cytotoxic properties of OXPL as well as 5-Fu on HCT-116 carcinoma cell lines, resulting in a cell viability of 4.61% for OXPL and 2.26% for 5-Fu. The previous findings strongly recommend the application of the synthetic CS/Di composite as carriers of numerous advantages, such as low cost, high natural reserves of raw materials, simple preparation, high and controlled loading capacity, biocompatibility, controlled release behavior, and significant enhancement of the cytotoxic effect of the drug on cancer cells. However, the introduced study is still within the limitations of the in vitro properties, and further biological in vivo studies are required to introduce a complete and realistic biological design for the composite as a delivery system.

4. EXPERIMENTAL WORK

4.1. Materials. The Central Metallurgical and Development Institute in Egypt provided a purified diatomite precursor. The composition of the material was 97.87% SiO_2, 1.79% Al_2O_3, and 0.34% L.O.I. Hydrogen peroxide (30%) and hydrochloric acid (37%), used in the leaching experiments, were obtained from Cornel Lab Company in Egypt. The deacetylation form of chitosan biopolymer with a molecular weight of 120,000 and 85% purity, as well as analytical grade acetic acid with a purity of 99.8%, was purchased from Sigma-Aldrich, Egypt, and used in the synthesis of the composite. 5-Fluorouracil (5-fluoro-1*H*,3*H*-pyrimidine-2,4-dione) and oxaliplatin with the molecular formula ([SP-4−2-(1*R*-trans)]-(1,2-cyclohexanediamine-*N*,*N*′)[ethanedioata(2--)-*O*,*O*′]-platinum) (397.29 MW) were obtained from Sigma-Aldrich Company in Egypt. 5-Fluorouracil was of analytical grade and had a purity of over 99%.

4.2. Synthesis Procedures of the Chitosan/Diatomite Composite (CS/Di). The diatomite powder was subjected to two steps of purification by leaching that were aimed at removing contaminants that had been detected in the raw samples. The first stage entailed the elimination of metallic impurities, which was accomplished by dispersing 5 g of diatomite precursor in diluted hydrochloric acid (10%) for 4 h at 100 °C under continuous mixing employing a magnetic stirrer. Following that, the removal of existing organic contaminants was accomplished by washing the hydrochloric-treated diatomite via H_2O_2 for approximately 5 h, 3 times. To remove any leftover H_2O_2, we washed the chemically refined diatomite many times with distilled water. As part of the subsequent processing step, the sample was subjected to an overnight drying process that occurred in an oven at a temperature of 80 °C. Following that, a homogeneous diatomite slurry was created by dispersing 3 g of the chemically refined diatomite in 50 mL of distilled water and sonicating the mixture (240 W) for 120 min. In a separate phase, 3 g of the powdered chitosan was immersed in 50 mL of a solution of acetic acid (0.1 M) and gently introduced to the diatomite mixture. For 12 h, the mixture was mixed using sonication vibrations (240 W) and magnetic stirring (800 rpm). After 12 h, the produced composite was completely washed, filtrated to eliminate the remaining acid, and dried overnight at 60 °C for characterization as well as application tests.

4.3. Characterization Techniques. An Empyrean PANalytical diffractometer was used to examine the X-ray diffraction (XRD) patterns of siliceous diatomite powder as well as its based composite. The rate of scanning had been set to 5°/min, and the voltage at which it operated was calibrated to 40 kV. The FTIR spectra were analyzed to evaluate the expected variations in the dominant chemical groups. The spectra were acquired by a Bruker Vertex 70 spectrometer with a frequency spectrum ranging from 400 to 4000 cm^{-1}. The predicted morphological changes have been investigated using images obtained from a Zeiss-Ultra 55 Gemini scanning electron microscope. HRTEM images taken with a JEOL-JEM2100 transmission electron microscope were used to investigate the interior structure and features. The surface area analyzer Beckman Coulter SA3100 was used in the investigation to determine the distinctive surface area and distribution of pore sizes using the BET and BJH methods, respectively.

4.4. Loading Experiments. The loading properties of CS/Di as a potential carrier of the two medications have been evaluated based on the effects of experimental loading conditions, such as pH (between 3 and 8), loading interval (1 to 24 h), concentration of drug (between 100 and 800 mg/L), and temperature (between 20 and 40 °C). Using a vortex rotator device, we uniformly blended the CS/Di particles with the OXPL and 5-Fu solutions. After the loading processes, Whatman filter paper was used to separate the drug-containing CS/Di particles from both the OXPL and 5-Fu-tested solutions. A ultraviolet−visible (UV−vis) spectrophotometer was employed to measure the concentrations of the two medications in the filtrates at wavelengths of 266 nm (5-Fu) and 209 nm (OXPL). The loading capacities were calculated using eq 15, considering the determined drug concentrations in the filtrates. The loading experiments were carried out in triplicate, and all of the computations and curves were displayed by using the average values that resulted from those tests.

$$\text{loaded drug (mg/g)} = \frac{(C_{\text{initial}} - C_{\text{residual}}) \times V_{\text{solvent}}}{\text{Wt}_{\text{carrier}}} \quad (15)$$

where C_{initial}, C_{residual}, V_{solvent}, and $\text{Wt}_{\text{carrier}}$ are the initial concentration, residual concentration, solvent volume, and carrier weight, respectively.

4.5. In Vitro Release Experiments. The study examined the release characteristics of the two medications from CS/Di particles based on regulated circumstances while taking 37.5

https://doi.org/10.1021/acsomega.3c04750
ACS Omega 2023, 8, 38330−38344

°C as the release temperature. The acetate buffering solution (pH 5.5) and the saline solution with phosphate buffer (pH 7.4) were employed to follow the expected release behaviors of OXPL. During the release of 5-Fu, the other two buffering solutions were administered (gastric fluid with a pH of 1.2 and intestinal fluid with a pH of 7.4). Predetermined quantities of CS/Di particles with specific dosages (100 mg/g) of OXPL and 5-Fu were dispersed individually inside 500 mL of the different evaluated buffers and homogenized up to 150 h via a DISTEK dissolution apparatus at a vessel revolving speed of 200 rpm. Five mL of the buffering solutions was periodically taken out of the device vessels during their mixing operation to measure the amounts of liberated OXPL and 5-Fu. A UV−visible spectrophotometer was used to perform this at maximum wavelengths of 266 nm (5-Fu) and 209 nm (OXPL). To keep the buffer volume consistent throughout the in vitro diffusion periods, a 5 mL sample of the buffers was returned to the vessels that contained the bulk buffers after each drug measurement cycle. The release tests were run 3 times, and the average values from those three runs were used for computations as well as graphing. The obtained concentrations of the two medications were applied to follow the percentages of the desorbed and diffused drugs based on the calculation indicated by eq 16.

$$\text{drug release (\%)} = \frac{\text{the amount of released drug}}{\text{amount of loaded drug}} \times 100 \quad (16)$$

4.6. In Vitro Cytotoxicity. *4.6.1. Cell Lines and Reagents.* Colorectal tumor cell lines (HCT-116; ATCC, Rockville, MD), buffer solution of HEPES, dimethyl sulfoxide with 99% purity (DMSO), DMEM, 0.25% of Trypsin−EDTA, 99% pure standard of 3(4, 5-dimethylthiazol-2-yl)-2.5 bromide (MTT), RPMI-1640, and fetal bovine serum were applied as required reagents to complete the in vitro cytotoxic tests of free CS/Di (unloaded) as well as drug-encapsulated CS/Di.

4.6.2. In Vitro Cytotoxic Effects. HCT-116 cell lines were initially cultivated in a medium made up of RPMI-1640 containing 50 g/mL gentamycin and 10% fetal calf serum. The cells were grown under specified humidity (5% CO_2) and temperature (37 °C) conditions. Three times each week, the HCT-116 cells were cultured before being suspended at a density of 5×10^4 cells per well in Corning-96-well plates and left to incubate for 24 h. Following a 24 h incubation period, specific amounts of free CS/Di, CS/Di loaded with OXPL, and CS/Di loaded with 5-Fu were administered to the culture plates. The MTT test was used to measure the cellular viability and proliferation of cancer cells under examination. Following a 48 h incubation stage, the culture medium was replaced with freshly prepared RPMI-1640 media (100 μL) and consequently mixed with the MTT reagent (10 μL; 12 mM). After the last incubation time of 5 h, formazan that had been created was seen to have a purple hue and was ultimately dissolved with 50 μL of DMSO. A microplate reader operating at a wavelength of 590 nm was used to measure the optical density of the treated cells that were incubated. Next, using eq 17, the cell viability percentages were determined.

$$\text{cell viability (\%)} = \frac{\text{mean OD}}{\text{control OD}} \times 100 \quad (17)$$

AUTHOR INFORMATION

Corresponding Authors

Wail Al Zoubi − *Materials Electrochemistry Laboratory, School of Materials Science and Engineering, Yeungnam University, Gyeongsan 38541, Republic of Korea;* orcid.org/0000-0003-4213-8481; Email: wailalzoubi@ynu.ac.kr

Mostafa R. Abukhadra − *Materials Technologies and their Applications Lab, Geology Department, Faculty of Science, Beni-Suef University, Beni-Suef 62511, Egypt; Geology Department, Faculty of Science, Beni-Suef University, Beni-Suef 65211, Egypt;* orcid.org/0000-0001-5404-7996; Email: Abukhadra89@Science.bsu.edu.eg

Authors

Haifa E. Alfassam − *Biology Department, College of Science, Princess Nourah bint Abdulrahman University, Riyadh 11671, Saudi Arabia*

Sarah I. Othman − *Biology Department, College of Science, Princess Nourah bint Abdulrahman University, Riyadh 11671, Saudi Arabia*

May N. Bin Jumah − *Biology Department, College of Science, Princess Nourah bint Abdulrahman University, Riyadh 11671, Saudi Arabia*

Maha A. Al-Waili − *Biology Department, College of Science, Princess Nourah bint Abdulrahman University, Riyadh 11671, Saudi Arabia*

Ahmed A. Allam − *Zoology Department, Faculty of Science, Beni-Suef University, Beni-Suef 62511, Egypt*

Complete contact information is available at: https://pubs.acs.org/10.1021/acsomega.3c04750

Author Contributions

This article was written through the contributions of all authors. All authors have given approval to the final version of the manuscript

Notes

The authors declare no competing financial interest.

ACKNOWLEDGMENTS

This work was funded by the Deanship of Scientific Research at Princess Nourah bint Abdulrahman University through the Research Groups Program Grant no. RGP-1443-0042.

REFERENCES

(1) El-Zeiny, H. M.; Abukhadra, M. R.; Sayed, O. M.; Osman, A. H. M.; Ahmed, S. A. Insight into Novel β-Cyclodextrin-Grafted-Poly (N-Vinylcaprolactam) Nanogel Structures as Advanced Carriers for 5-Fluorouracil: Equilibrium Behavior and Pharmacokinetic Modeling. *Colloids Surf., A* **2020**, *586*, No. 124197, DOI: 10.1016/j.colsurfa.2019.124197.

(2) Cutrim, E. S. M.; Vale, A. A. M.; Manzani, D.; Barud, H. S.; Rodríguez-Castellón, E.; Santos, A. P. S. A.; Alcântara, A. C. S. Preparation, Characterization and in Vitro Anticancer Performance of Nanoconjugate Based on Carbon Quantum Dots and 5-Fluorouracil. *Mater. Sci. Eng.: C* **2021**, *120*, No. 111781, DOI: 10.1016/j.msec.2020.111781.

(3) Sayed, M. A.; El-Zeiny, H. M.; Khim, J. S.; Ajarem, J. S.; Allam, A. A.; Abukhadra, M. R. Insight into the Loading Properties of Na+ Green-Functionalized Clinoptilolite as a Potential Carrier for the 5-Fluorouracil Drug, Its Release Kinetics, and Cytotoxicity. *ACS Omega* **2022**, *7* (8), 6991−7001.

(4) Abuzar, S. M.; Park, E. J.; Seo, Y.; Lee, J.; Baik, S. H.; Hwang, S.-J. Preparation and Evaluation of Intraperitoneal Long-Acting

https://doi.org/10.1021/acsomega.3c04750
ACS Omega 2023, 8, 38330−38344

Oxaliplatin-Loaded Multi-Vesicular Liposomal Depot for Colorectal Cancer Treatment. *Pharmaceutics* **2020**, *12* (8), No. 736, DOI: 10.3390/pharmaceutics12080736.
(5) Sundaramoorthy, P.; Ramasamy, T.; Mishra, S. K.; Jeong, K.-Y.; Yong, C. S.; Kim, J. O.; Kim, H. M. Engineering of Caveolae-Specific Self-Micellizing Anticancer Lipid Nanoparticles to Enhance the Chemotherapeutic Efficacy of Oxaliplatin in Colorectal Cancer Cells. *Acta Biomater.* **2016**, *42*, 220−231.
(6) Othman, S. I.; Allam, A. A.; Al Fassam, H.; Abu-Taweel, G. M.; Altoom, N.; Abukhadra, M. R. Sonoco Green Decoration of Clinoptilolite with MgO Nanoparticles as a Potential Carrier for 5-Fluorouracil Drug: Loading Behavior, Release Profile, and Cytotoxicity. *J. Inorg. Organomet. Polym. Mater.* **2021**, *31* (12), 4608−4622.
(7) Tian, L.; Abukhadra, M. R.; Mohamed, A. S.; Nadeem, A.; Ahmad, S. F.; Ibrahim, K. E. Insight into the Loading and Release Properties of an Exfoliated Kaolinite/Cellulose Fiber (EXK/CF) Composite as a Carrier for Oxaliplatin Drug: Cytotoxicity and Release Kinetics. *ACS Omega* **2020**, *5* (30), 19165−19173.
(8) Yang, T.; Huang, J.; Wang, Y.; Zheng, A.; Shu, Y.; Wang, J. β-Cyclodextrin-Decorated Carbon Dots Serve as Nanocarriers for Targeted Drug Delivery and Controlled Release. *ChemNanoMat* **2019**, *5* (4), 479−487.
(9) Li, Y.; Sun, Z.; Cui, Y.; Zhang, H.; Zhang, S.; Wang, X.; Liu, S.; Gao, Q. Oxaliplatin Derived Monofunctional Triazole-Containing Platinum(II) Complex Counteracts Oxaliplatin-Induced Drug Resistance in Colorectal Cancer. *Bioorg. Chem.* **2021**, *107*, No. 104636, DOI: 10.1016/j.bioorg.2021.104636.
(10) Tummala, S.; Kumar, M. N. S.; Prakash, A. Formulation and Characterization of 5-Fluorouracil Enteric Coated Nanoparticles for Sustained and Localized Release in Treating Colorectal Cancer. *Saudi Pharm. J.* **2015**, *23* (3), 308−314, DOI: 10.1016/j.jsps.2014.11.010.
(11) Wan, W.; Ouyang, H.; Jiang, Z.; Cui, Y.; Li, J.; He, M.; Yang, S.; Zhang, X.; Feng, Y.; Wei, Y. Synthesis and Intracellular Drug Delivery Applications of Hyperbranched Polymers Functionalized β-Cyclodextrin. *Colloid Interface Sci. Commun.* **2021**, *42*, No. 100425, DOI: 10.1016/j.colcom.2021.100425.
(12) Wang, J.; Guo, Z.; Xiong, J.; Wu, D.; Li, S.; Tao, Y.; Qin, Y.; Kong, Y. Facile Synthesis of Chitosan-Grafted Beta-Cyclodextrin for Stimuli-Responsive Drug Delivery. *Int. J. Biol. Macromol.* **2019**, *125*, 941−947.
(13) Chang, C.-W.; Lee, H.-C.; Li, L.-H.; Chiang Chiau, J.-S.; Wang, T.-E.; Chuang, W.-H.; Chen, M.-J.; Wang, H.-Y.; Shih, S.-C.; Liu, C.-Y.; Tsai, T.-H.; Chen, Y.-J. Fecal Microbiota Transplantation Prevents Intestinal Injury, Upregulation of Toll-Like Receptors, and 5-Fluorouracil/Oxaliplatin-Induced Toxicity in Colorectal Cancer. *Int. J. Mol. Sci.* **2020**, *21* (2), No. 386, DOI: 10.3390/ijms21020386.
(14) Tan, D.; Yuan, P.; Dong, F.; He, H.; Sun, S.; Liu, Z. Selective Loading of 5-Fluorouracil in the Interlayer Space of Methoxy-Modified Kaolinite for Controlled Release. *Appl. Clay Sci.* **2018**, *159*, 102−106.
(15) Wei, T.-T.; Lin, Y.-T.; Tang, S.-P.; Luo, C.-K.; Tsai, C.-T.; Shun, C.-T.; Chen, C.-C. Metabolic Targeting of HIF-1α Potentiates the Therapeutic Efficacy of Oxaliplatin in Colorectal Cancer. *Oncogene* **2020**, *39* (2), 414−427.
(16) Han, W.; Yin, H.; Ma, H.; Wang, Y.; Kong, D.; Fan, Z. Curcumin Regulates ERCC1 Expression and Enhances Oxaliplatin Sensitivity in Resistant Colorectal Cancer Cells through Its Effects on miR-409−3p. *Evidence-Based Complementary Altern. Med.* **2020**, *2020*, No. 8394574, DOI: 10.1155/2020/8394574.
(17) Zhang, N.; Yin, Y.; Xu, S.-J.; Chen, W.-S. 5-Fluorouracil: Mechanisms of Resistance and Reversal Strategies. *Molecules* **2008**, *13* (8), 1551−1569.
(18) Martínez, E.; Osorio, M.; Finkielstein, C.; Ortíz, I.; Peresin, M. S.; Castro, C. 5-Fluorouracil Drug Delivery System Based on Bacterial Nanocellulose for Colorectal Cancer Treatment: Mathematical and in Vitro Evaluation. *Int. J. Biol. Macromol.* **2022**, *220*, 802−815.
(19) Dey, D. K.; Chang, S. N.; Vadlamudi, Y.; Park, J. G.; Kang, S. C. Synergistic Therapy with Tangeretin and 5-Fluorouracil Accelerates the ROS/JNK Mediated Apoptotic Pathway in Human Colorectal Cancer Cell. *Food Chem. Toxicol.* **2020**, *143*, No. 111529, DOI: 10.1016/j.fct.2020.111529.
(20) Lee, J. H.; Kim, W. Involvement of Serotonergic System in Oxaliplatin-Induced Neuropathic Pain. *Biomedicines* **2021**, *9* (8), No. 970, DOI: 10.3390/biomedicines9080970.
(21) dos Santos, G. G. L.; Oliveira, A. L. L.; Santos, D. S.; do Espírito Santo, R. F.; Silva, D. N.; Juiz, P. J. L.; Soares, M. B. P.; Villarreal, C. F. Mesenchymal Stem Cells Reduce the Oxaliplatin-Induced Sensory Neuropathy through the Reestablishment of Redox Homeostasis in the Spinal Cord. *Life Sci.* **2021**, *265*, No. 118755, DOI: 10.1016/j.lfs.2020.118755.
(22) Altoom, N.; Ibrahim, S. M.; Othman, S. I.; Allam, A. A.; Alqhtani, H. A.; Al-Otaibi, F. S.; Abukhadra, M. R. Characterization of β-Cyclodextrin/Phillipsite (β-CD/Ph) Composite as a Potential Carrier for Oxaliplatin as Therapy for Colorectal Cancer; Loading, Release, and Cytotoxicity. *Colloids Surf., A* **2022**, *648*, No. 129144, DOI: 10.1016/j.colsurfa.2022.129144.
(23) Abukhadra, M. R.; Refay, N. M.; El-Sherbeeny, A. M.; Mostafa, A. M.; Elmeligy, M. A. Facile Synthesis of Bentonite/Biopolymer Composites as Low-Cost Carriers for 5-Fluorouracil Drug; Equilibrium Studies and Pharmacokinetic Behavior. *Int. J. Biol. Macromol.* **2019**, *141*, 721−731.
(24) Shad, P. M.; Karizi, S. Z.; Javan, R. S.; Mirzaie, A.; Noorbazargan, H.; Akbarzadeh, I.; Rezaie, H. Folate Conjugated Hyaluronic Acid Coated Alginate Nanogels Encapsulated Oxaliplatin Enhance Antitumor and Apoptosis Efficacy on Colorectal Cancer Cells (HT29 Cell Line). *Toxicol. In Vitro* **2020**, *65*, No. 104756, DOI: 10.1016/j.tiv.2019.104756.
(25) Bandi, S. P.; Venuganti, V. V. K. Functionalized Polymeric Patch for Localized Oxaliplatin Delivery to Treat Gastric Cancer. *Mater. Sci. Eng.: C* **2021**, *128*, No. 112302, DOI: 10.1016/j.msec.2021.112302.
(26) Li, W.; Han, F.; Liu, H.; Niu, X.; Shi, L. RETRACTED: The Synthesis of Sulfate Doped Hydroxyapatite for Enhanced Drug Loading and Chemotherapeutic Drug Delivery towards Lung Cancer Treatment. *Ceram. Int.* **2020**, *46* (18), 28578−28584.
(27) Alyassin, Y.; Sayed, E. G.; Mehta, P.; Ruparelia, K.; Arshad, M. S.; Rasekh, M.; Shepherd, J.; Kucuk, I.; Wilson, P. B.; Singh, N.; Chang, M.-W.; Fatouros, D. G.; Ahmad, Z. Application of Mesoporous Silica Nanoparticles as Drug Delivery Carriers for Chemotherapeutic Agents. *Drug Discovery Today* **2020**, *25* (8), 1513−1520.
(28) Ibrahim, S. M.; Jumah, M. N. B.; Othman, S. I.; Alruhaimi, R. S.; Al-Khalawi, N.; Salama, Y. F.; Allam, A. A.; Abukhadra, M. R. Synthesis of Chitosan/Diatomite Composite as an Advanced Delivery System for Ibuprofen Drug; Equilibrium Studies and the Release Profile. *ACS Omega* **2021**, *6* (20), 13406−13416, DOI: 10.1021/acsomega.1c01514.
(29) Rehman, F.; Ahmed, K.; Rahim, A.; Muhammad, N.; Tariq, S.; Azhar, U.; Khan, A. J.; us Sama, Z.; Volpe, P. L. O.; Airoldi, C. Organo-Bridged Silsesquioxane Incorporated Mesoporous Silica as a Carrier for the Controlled Delivery of Ibuprofen and Fluorouracil. *J. Mol. Liq.* **2018**, *258*, 319−326.
(30) Fan, H.-B.; Ren, Q.-F.; Wang, S.-L.; Jin, Z.; Ding, Y. Synthesis of the Ag/Ag3PO4/Diatomite Composites and Their Enhanced Photocatalytic Activity Driven by Visible Light. *J. Alloys Compd.* **2019**, *775*, 845−852.
(31) Chen, Z.; Zhang, H.; Fan, G.; He, X.; He, Z.; Zhang, L. Diatomite Composited with a Zeolitic Imidazolate Framework for Removing Phosphate from Water. *ACS Omega* **2022**, *7* (30), 26154−26164.
(32) AbuKhadra, M. R.; Eid, M. H.; Allam, A. A.; Ajarem, J. S.; Almalki, A. M.; Salama, Y. Evaluation of Different Forms of Egyptian Diatomite for the Removal of Ammonium Ions from Lake Qarun: A Realistic Study to Avoid Eutrophication. *Environ. Pollut.* **2020**, *266*, No. 115277, DOI: 10.1016/j.envpol.2020.115277.
(33) Li, K.; Hu, Z.; Zhao, R.; Zhou, J.; Jing, C.; Sun, Q.; Rao, J.; Yao, K.; Dong, B.; Liu, X.; Li, H.; Zhang, Y.; Ji, J. A Multidimensional Rational Design of Nickel−Iron Sulfide and Carbon Nanotubes on

Diatomite via Synergistic Modulation Strategy for Supercapacitors. *J. Colloid Interface Sci.* **2021**, *603*, 799−809.
(34) Kong, X.; Yu, Q.; Li, E.; Wang, R.; Liu, Q.; Wang, A. Diatomite Photonic Crystals for Facile On-Chip Chromatography and Sensing of Harmful Ingredients from Food. *Materials* **2018**, *11* (4), No. 539, DOI: 10.3390/ma11040539.
(35) Wu, S.; Wang, C.; Jin, Y.; Zhou, G.; Zhang, L.; Yu, P.; Sun, L. Green Synthesis of Reusable Super-Paramagnetic Diatomite for Aqueous Nickel (II) Removal. *J. Colloid Interface Sci.* **2021**, *582*, 1179−1190.
(36) Janićijević, J.; Krajišnik, D.; Čalija, B.; Dobričić, V.; Daković, A.; Krstić, J.; Marković, M.; Milić, J. Inorganically Modified Diatomite as a Potential Prolonged-Release Drug Carrier. *Mater. Sci. Eng.: C* **2014**, *42*, 412−420.
(37) Zhang, H.; Shahbazi, M.-A.; Mäkilä, E. M.; da Silva, T. H.; Reis, R. L.; Salonen, J. J.; Hirvonen, J. T.; Santos, H. A. Diatom Silica Microparticles for Sustained Release and Permeation Enhancement Following Oral Delivery of Prednisone and Mesalamine. *Biomaterials* **2013**, *34* (36), 9210−9219.
(38) Janićijević, J.; Milić, J.; Čalija, B.; Micov, A.; Stepanović-Petrović, R.; Tomić, M.; Daković, A.; Dobričić, V.; Vasiljević, B. N.; Krajišnik, D. Potentiation of the Ibuprofen Antihyperalgesic Effect Using Inorganically Functionalized Diatomite. *J. Mater. Chem. B* **2018**, *6* (36), 5812−5822, DOI: 10.1039/C8TB01376D.
(39) Saleh, T. A.; Tuzen, M.; Sarı, A. Evaluation of Poly(Ethylene Diamine-Trimesoyl Chloride)-Modified Diatomite as Efficient Adsorbent for Removal of Rhodamine B from Wastewater Samples. *Environ. Sci. Pollut. Res.* **2021**, *28* (39), 55655−55666.
(40) Liu, G.; Abukhadra, M. R.; El-Sherbeeny, A. M.; Mostafa, A. M.; Elmeligy, M. A. Insight into the Photocatalytic Properties of diatomite@Ni/NiO Composite for Effective Photo-Degradation of Malachite Green Dye and Photo-Reduction of Cr (VI) under Visible Light. *J. Environ. Manage.* **2020**, *254*, No. 109799, DOI: 10.1016/j.jenvman.2019.109799.
(41) Zhao, Y.; Tian, G.; Duan, X.; Liang, X.; Meng, J.; Liang, J. Environmental Applications of Diatomite Minerals in Removing Heavy Metals from Water. *Ind. Eng. Chem. Res.* **2019**, *58* (27), 11638−11652.
(42) Dizaji, B. F.; Azerbaijan, M. H.; Sheisi, N.; Goleij, P.; Mirmajidi, T.; Chogan, F.; Irani, M.; Sharafian, F. Synthesis of PLGA/Chitosan/Zeolites and PLGA/Chitosan/Metal Organic Frameworks Nanofibers for Targeted Delivery of Paclitaxel toward Prostate Cancer Cells Death. *Int. J. Biol. Macromol.* **2020**, *164*, 1461−1474, DOI: 10.1016/j.ijbiomac.2020.07.228.
(43) Dai, H.; Huang, Y.; Zhang, Y.; Zhang, H.; Huang, H. Green and Facile Fabrication of Pineapple Peel Cellulose/Magnetic Diatomite Hydrogels in Ionic Liquid for Methylene Blue Adsorption. *Cellulose* **2019**, *26* (6), 3825−3844.
(44) Saad, A. M.; Abukhadra, M. R.; Ahmed, S. A.-K.; Elzanaty, A. M.; Mady, A. H.; Betiha, M. A.; Shim, J.-J.; Rabie, A. M. Photocatalytic Degradation of Malachite Green Dye Using Chitosan Supported ZnO and Ce−ZnO Nano-Flowers under Visible Light. *J. Environ. Manage.* **2020**, *258*, No. 110043, DOI: 10.1016/j.jenvman.2019.110043.
(45) Jiang, Y.; Abukhadra, M. R.; Refay, N. M.; Sharaf, M. F.; El-Meligy, M. A.; Awwad, E. M. Synthesis of Chitosan/MCM-48 and β-Cyclodextrin/MCM-48 Composites as Bio-Adsorbents for Environmental Removal of Cd^{2+} Ions; Kinetic and Equilibrium Studies. *React. Funct. Polym.* **2020**, *154*, No. 104675, DOI: 10.1016/j.reactfunctpolym.2020.104675.
(46) Narmani, A.; Kamali, M.; Amini, B.; Salimi, A.; Panahi, Y. Targeting Delivery of Oxaliplatin with Smart PEG-Modified PAMAM G4 to Colorectal Cell Line: In Vitro Studies. *Process Biochem.* **2018**, *69*, 178−187.
(47) Lenz, K.; Hann, S.; Koellensperger, G.; Stefanka, Z.; Stingeder, G.; Weissenbacher, N.; Mahnik, S. N.; Fuerhacker, M. Presence of Cancerostatic Platinum Compounds in Hospital Wastewater and Possible Elimination by Adsorption to Activated Sludge. *Sci. Total Environ.* **2005**, *345* (1−3), 141−152.
(48) Abukhadra, M. R.; Allah, A. F. Synthesis and Characterization of Kaolinite Nanotubes (KNTs) as a Novel Carrier for 5-Fluorouracil of High Encapsulation Properties and Controlled Release. *Inorg. Chem. Commun.* **2019**, *103*, 30−36.
(49) Salam, M. A.; Abukhadra, M. R.; Mostafa, M. Effective Decontamination of As(V), Hg(II), and U(VI) Toxic Ions from Water Using Novel Muscovite/Zeolite Aluminosilicate Composite: Adsorption Behavior and Mechanism. *Environ. Sci. Pollut. Res.* **2020**, *27* (12), 13247−13260.
(50) Ashraf, M.-T.; AlHammadi, A. A.; El-Sherbeeny, A. M.; Alhammadi, S.; Al Zoubi, W.; Ko, Y. G.; Abukhadra, M. R. Synthesis of Cellulose Fibers/Zeolite-A Nanocomposite as an Environmental Adsorbent for Organic and Inorganic Selenium Ions; Characterization and Advanced Equilibrium Studies. *J. Mol. Liq.* **2022**, *360*, No. 119573, DOI: 10.1016/j.molliq.2022.119573.
(51) Lin, X.; Xie, Y.; Lu, H.; Xin, Y.; Altaf, R.; Zhu, S.; Liu, D. Facile Preparation of Dual La-Zr Modified Magnetite Adsorbents for Efficient and Selective Phosphorus Recovery. *Chem. Eng. J.* **2021**, *413*, No. 127530, DOI: 10.1016/j.cej.2020.127530.
(52) Albukhari, S. M.; Salam, M. A.; Abukhadra, M. R. Effective Retention of Inorganic Selenium Ions (Se (VI) and Se (IV)) Using Novel Sodalite Structures from Muscovite; Characterization and Mechanism. *J. Taiwan Inst. Chem. Eng.* **2021**, *120*, 116−126.
(53) Huang, Y.; Li, S.; Chen, J.; Zhang, X.; Chen, Y. Adsorption of Pb(II) on Mesoporous Activated Carbons Fabricated from Water Hyacinth Using H_3PO_4 Activation: Adsorption Capacity, Kinetic and Isotherm Studies. *Appl. Surf. Sci.* **2014**, *293*, 160−168.
(54) Dinu, M. V.; Lazar, M. M.; Dragan, E. S. Dual Ionic Cross-Linked Alginate/Clinoptilolite Composite Microbeads with Improved Stability and Enhanced Sorption Properties for Methylene Blue. *React. Funct. Polym.* **2017**, *116*, 31−40.
(55) Selim, A. Q.; Mohamed, E. A.; Mobarak, M.; Zayed, A. M.; Seliem, M. K.; Komarneni, S. Cr(VI) Uptake by a Composite of Processed Diatomite with MCM-41: Isotherm, Kinetic and Thermodynamic Studies. *Microporous Mesoporous Mater.* **2018**, *260*, 84−92.
(56) Yang, X.; Wang, J.; El-Sherbeeny, A. M.; AlHammadi, A. A.; Park, W.-H.; Abukhadra, M. R. Insight into the Adsorption and Oxidation Activity of a ZnO/Piezoelectric Quartz Core-Shell for Enhanced Decontamination of Ibuprofen: Steric, Energetic, and Oxidation Studies. *Chem. Eng. J.* **2022**, *431*, No. 134312, DOI: 10.1016/j.cej.2021.134312.
(57) Mobarak, M.; Ali, R. A. M.; Seliem, M. K. Chitosan/Activated Coal Composite as an Effective Adsorbent for Mn(VII): Modeling and Interpretation of Physicochemical Parameters. *Int. J. Biol. Macromol.* **2021**, *186*, 750−758.
(58) Singh, T.; Kang, D. H.; Kim, T. W.; Kong, H. J.; Ryu, J. S.; Jeon, S.; Ahn, T. S.; Jeong, D.; Baek, M. J.; Im, J. Intracellular Delivery of Oxaliplatin Conjugate via Cell Penetrating Peptide for the Treatment of Colorectal Carcinoma in Vitro and in Vivo. *Int. J. Pharm.* **2021**, *606*, No. 120904, DOI: 10.1016/j.ijpharm.2021.120904.
(59) Abukhadra, M. R.; Refay, N. M.; Nadeem, A.; El-Sherbeeny, A. M.; Ibrahim, K. E. Insight into the Role of Integrated Carbohydrate Polymers (Starch, Chitosan, and β-Cyclodextrin) with Mesoporous Silica as Carriers for Ibuprofen Drug; Equilibrium and Pharmacokinetic Properties. *Int. J. Biol. Macromol.* **2020**, *156*, 537−547.
(60) Abukhadra, M. R.; Refay, N. M.; El-Sherbeeny, A. M.; El-Meligy, M. A. Insight into the Loading and Release Properties of MCM-48/Biopolymer Composites as Carriers for 5-Fluorouracil: Equilibrium Modeling and Pharmacokinetic Studies. *ACS Omega* **2020**, *5* (20), 11745−11755.
(61) Sun, L.; Chen, Y.; Zhou, Y.; Guo, D.; Fan, Y.; Guo, F.; Zheng, Y.; Chen, W. Preparation of 5-Fluorouracil-Loaded Chitosan Nanoparticles and Study of the Sustained Release in Vitro and in Vivo. *Asian J. Pharm. Sci.* **2017**, *12* (5), 418−423.
(62) Ge, M.; Tang, W.; Du, M.; Liang, G.; Hu, G.; Alam, S. M. J. Research on 5-Fluorouracil as a Drug Carrier Materials with Its in

Vitro Release Properties on Organic Modified Magadiite. *Eur. J. Pharm. Sci.* **2019**, *130*, 44−53, DOI: 10.1016/j.ejps.2019.01.017.
(63) Lisik, A.; Musiał, W. Conductomeric Evaluation of the Release Kinetics of Active Substances from Pharmaceutical Preparations Containing Iron Ions. *Materials* **2019**, *12* (5), No. 730, DOI: 10.3390/ma12050730.
(64) Betsiou, M.; Bantsis, G.; Zoi, I.; Sikalidis, C. Adsorption and release of gemcitabine hydrochloride and oxaliplatin by hydroxyapatite. *Ceram. Int.* **2012**, *38* (4), 2719−2724.
(65) Altoom, N.; Ashraf, M. T.; Ibrahim, S. M.; Othman, S. I.; Allam, A. A.; Alqhtani, H. A.; Abukhadra, M. R. Insight into the loading, release, and anticancer properties of cellulose/zeolite-A as an enhanced delivery structure for oxaliplatin chemotherapy; characterization and mechanism. *J. Sol-Gel Sci. Technol.* **2022**, *103* (3), 752−765.
(66) Alfassam, H. E.; Ashraf, M. T.; Al Othman, S. I.; Al-Waili, M. A.; Allam, A. A.; Abukhadra, M. R. Synthesis and characterization of cellulose functionalized zeolitic diatomite as an enhanced carrier of oxaliplatin drug; loading, release, and cytotoxicity. *Int. J. Biol. Macromol.* **2023**, *235*, No. 123825, DOI: 10.1016/j.ijbiomac.2023.123825.
(67) Alfassam, H. E.; Al Othman, S. I.; Al-Waili, M. A.; Allam, A. A.; Abukhadra, M. R. Characterization of *β*-cyclodextrin Hybridized Diatomite as Potential Delivery Systems of Oxaliplatin and 5-Fluorouracil Drugs; Equilibrium Modeling of Loading and Release Kinetics. *J. Macromol. Sci., Part B* **2023**, *62* (9), 478−503.
(68) Çiftçi, H.; Arpa, M. D.; Gülaçar, İ.M.; Özcan, L.; Ersoy, B. Development and evaluation of mesoporous montmorillonite/magnetite nanocomposites loaded with 5-Fluorouracil. *Microporous Mesoporous Mater.* **2020**, *303*, No. 110253, DOI: 10.1016/j.micromeso.2020.110253.
(69) Datt, A.; Burns, E. A.; Dhuna, N. A.; Larsen, S. C. Loading and release of 5-fluorouracil from HY zeolites with varying SiO2/Al2O3 ratios. *Microporous Mesoporous Mater.* **2013**, *167*, 182−187.

https://doi.org/10.1021/acsomega.3c04750
ACS Omega 2023, 8, 38330−38344